Osteoarthritis and Cartilage Open 7 (2025) 100612

Contents lists available at ScienceDirect

Osteoarthritis and Cartilage Open

journal homepage: www.elsevier.com/journals/osteoarthritis-and-cartilage-open/2665-9131

Extracellular vesicles in osteoarthritis synovial fluid contain both transmembrane and intravesical TNF-α

Xin Zhang [a,b,*], Virginia Byers Kraus [a,b,c]

[a] Duke Molecular Physiology Institute, Duke University School of Medicine, Duke University, Durham, NC, USA
[b] Department of Orthopaedic Surgery, Duke University School of Medicine, Duke University, Durham, NC, USA
[c] Department of Medicine, Duke University School of Medicine, Duke University, Durham, NC, USA

ARTICLE INFO

Handling Editor: Professor H Madry

Keywords:
Flow cytometry
Knee osteoarthritis
Cytokine
TNF-α

ABSTRACT

Objective: We previously identified extracellular vesicles (EVs) as a key source of TNF-α in the plasma of both knee osteoarthritis (OA) patients and healthy individuals. Building on these findings, this study aimed to evaluate the presence of surface-bound transmembrane TNF-α (TM-TNF-α) and intravesical TNF-α in EVs from OA synovial fluid (SF).

Methods: Using high-resolution flow cytometry, we rigorously quantified the percentages and integrated mean fluorescence intensity (iMFI) of surface-bound, intravesical, and total TNF-α forms in EVs isolated from SF of 25 knee OA patients. CZ CELLxGENE and OA joint tissue-derived single-cell and single-nuclei RNA sequencing data were used to analyze *TNF* gene expression.

Results: TNF is expressed across multiple cell types. In OA joints it is predominantly expressed by synoviocytes, with TNF-α present in the SF EV pool. TM-TNF-α was consistently detected on SF EVs using three distinct TNF-α antibodies, although its frequency and iMFI were significantly lower than the corresponding intravesical TNF-α (Friedman test with Benjamini-Hochberg correction, FDR <0.05). The average percentages (and range) of EVs expressing TNF-α, as detected by the three anti-TNF-α antibodies, were 2.57 % (0.09–37.08 %) for TM-TNF-α^+, 8.62 % (0.38–43.64 %) for intravesical TNF-α^+, and 14.42 % (0.71–44.32 %) for total EV TNF-α^+. Interestingly, TM-TNF-α frequencies on SF EVs were similar to those observed on various immune cell subsets in peripheral blood.

Conclusions: While intravesical TNF-α may evade TNF-α inhibitors, TNF-α carried by EVs retains pathogenic potential, either by activating pro-inflammatory pathways via TM-TNF-α receptor engagement on target cells, or through the transfer of TNF-α cargo to recipient cells.

1. Introduction

Extracellular vesicles (EVs) are nanosized particles produced by nearly all mammalian cells. They carry surface markers and biological cargo such as mitochondria, messenger ribonucleic acids (RNAs), small non-coding RNAs (including miRNAs and piRNAs), cytokines and various proteins, reflective of their parent cells' condition [1–3]. EVs play a pivotal role in intercellular communication by delivering their cargo to recipient cells or by interacting through surface ligand-receptor interactions [2,4–7]. As such, they provide valuable insight into physiological and pathological states of the body, especially in aging and age-related diseases like osteoarthritis (OA) [1,7–12].

While many OA studies have focused primarily on small EVs (SEVs), often referred to as exosomes [8,9,13], our research focuses on EVs of all sizes [10,12,14], as evidence is insufficient to exclude the medium-sized EVs (MEVs) and large EVs (LEVs) from OA-related studies. We and others

Abbreviations: EV, extracellular vesicles; RNA, ribonucleic acid; OA, osteoarthritis; LEV, large EV; MEV, medium-sized EV; SEV, small EV; rOA, radiographic osteoarthritis; CD, Cluster of Differentiation; HLA, Human Leukocyte Antigen; CSPG4, Chondroitin Sulfate Proteoglycan 4; VSIG4, V-Set and Immunoglobulin Domain Containing 4; LRP1, low-density lipoprotein receptor-related protein 1; BGN, Biglycan; MARCO, Macrophage receptor MARCO; NRP1, Neuropilin-1; PTPRS, protein tyrosine phosphatase receptor type S; IL, Interleukin; TNF, Tumor Necrosis Factor; SF, synovial fluid; K/L, Kellgren Lawrence; TM-TNF-α, transmembrane TNF-α; TKR, total knee replacement; df-PBS, double filtered PBS; MFI, mean fluorescence intensity; iMFI, integrated mean fluorescence intensity; sc, single-cell; RNA-seq, RNA sequencing; sn, single-nuclei.

* Corresponding author. Duke University, Durham, NC 27701, USA.
E-mail address: xin.zhang193@duke.edu (X. Zhang).

https://doi.org/10.1016/j.ocarto.2025.100612
Received 21 October 2024; Accepted 4 April 2025

have demonstrated that EVs from OA patients carry a wide range of frequencies of surface markers (Cluster of Differentiation [CD] 81, CD9, CD63, CD29, CD4, CD8, CD68, CD14, CD56, CD15, CD19, CD235a, CD41a, CD34, CD31, Human Leukocyte Antigen [HLA]-ABC, HLA-G, HLA-DRDPDQ, Chondroitin Sulfate Proteoglycan 4 [CSPG4], V-Set and Immunoglobulin Domain Containing 4 [VSIG4], CD109, low-density lipoprotein receptor-related protein 1 [LRP1], Biglycan [BGN], CD163, Macrophage receptor MARCO [MARCO], Neuropilin-1 [NRP1] and protein tyrosine phosphatase receptor type S [PTPRS]), and cytokines (Interleukin [IL]-1β, IL-2, IL-4, IL-5, IL-6, IL-13, Tumor Necrosis Factor [TNF]-α, Interferon-γ, IL-11, IL17 A/F, IL-21, IL-22 and IL-27) [8–10,12–14]. Notably, OA-related EVs are associated with OA disease severity [12] and progression [10], induce M1 macrophages to produce pro-inflammatory cytokines, chemokines and metalloproteases [8], enhance chemotaxis of peripheral blood mononuclear cells, promote inflammatory responses, and inhibit chondrocyte proliferation [13].

We identified EVs as a major source of TNF-α in plasma from both knee OA patients and healthy individuals, with higher concentrations of TNF-α in EVs than matched EV-depleted supernatants [3,14]. Moreover, TNF-α concentrations in plasma EVs were significantly correlated with that of the matched synovial fluid (SF) EVs, suggesting active migration of these EVs between plasma and SF [14]. TNF-α^+ plasma EVs of all sizes, particularly TNF-α^+ MEVs and SEVs, predict knee radiographic OA (rOA) progression [10]. Compared to plasma EVs, SF-derived EVs are more proximal indicators of OA pathology, and contain higher amounts of pathogenic factors, such as TNF-α [12,14], especially in more advanced rOA (Kellgren Lawrence [K/L] grade 3–4) [9]. This highlights the role of TNF-α^+ EVs in OA progression. Another recent study found that LEVs from TNF-α-treated natural killer cells enhanced the phagocytic activity, oxidative burst, and expression of key immune mediators (CD71, TLR4 and HLA-DR) by THP-1 cells, with effects surpassing those of direct TNF-α treatment [15]. This suggests that TNF-α^+ EVs play a critical pathogenic role in OA, amplifying inflammatory and immune responses.

Although TNF-α inhibitors have shown therapeutic promise in diseases, like rheumatoid arthritis [16], and preclinical studies in OA (3 human *in vitro*, 2 animal *in vitro*, and 8 animal *in vivo* studies) [17–30], no benefits have been observed in six completed clinical trials in OA reported in clinicaltrials.gov (search 9/27/2024) that used either adalimumab (three trials for hand OA and two trials for knee OA), or infliximab (one trial for knee OA). We hypothesize that the ineffectiveness of TNF-α inhibitors in OA is due to the sequestration of pathogenic TNF-α within EVs, making it less accessible to the inhibitors [10]. The transmembrane form of TNF-α (TM-TNF-α) that acts as both ligand and receptor [16,31–33], and its soluble form, play critical roles in inflammation [32,34], but their involvement in EVs remains unclear. Anti-TNF agents neutralize soluble TNF-α by binding to it; their effects on TM-TNF-α and TNF-α-producing cells differ from effects on soluble TNF-α in terms of affinity, and avidity [16,32,35]. Additionally, their effects on TNF-α-carrying EVs remain undefined. This study aims to quantify TM-TNF-α and intravesical TNF-α within EVs from the SF of knee OA patients, potentially elucidating new mechanisms behind the role of TNF-α in OA pathology.

2. Methods

2.1. SF EV isolation

All SF samples were derived as anonymized waste specimens under the approval of the Institutional Review Board of Duke University. Fifteen samples were acquired in the clinic at the time of therapeutic aspiration of effusion of individuals with knee rOA. Ten samples were acquired at the time of total knee replacement (TKR) for OA with the OA determination based on the stated surgical indication for the procedure. The total 25 OA patients had mean age 66 ± 11 years, range 46–88 years and were 60 % female. As previously described [12,14], SF specimens were centrifuged at 3000 rpm for 15 min at 4 °C on the day of collection to remove cells and debris, then aliquoted and frozen at −80 °C until analysis. All SF specimens were light yellow and free of blood contamination. For EV isolation, frozen SF was thawed, centrifuged at 2000 g for 10 min at 4 °C to remove any debris, then digested with hyaluronidase (10 unit/ml, Sigma-Aldrich) for 1 h at 37 °C in a ThermoMixer C dry block (Eppendorf) with shaking at 300 rpm. The hyaluronidase-digested SF, in 30 μl volumes utilized for each flow cytometry panel, was washed with 200 μl of double filtered (df)-PBS (filtered twice through a 100 nm filter [EMD Millipore]) followed by EV isolation by ultrafiltration using Vivaspin Centrifugal Filters (Sartorius) with a 100 kDa cut-off (pore size 10 nm) that retained EVs while removing many proteins [1,36–38], then profiled using high-resolution multicolor flow cytometry.

2.2. High-resolution multicolor flow cytometry

Unstained fractions of SF, both EV-enriched and EV-depleted, were used for counting numbers of EVs. As previously reported [12], for EV surface marker statining, SF EV pellets were resuspended in df-PBS and stained with fluorescence-conjugated antibodies against human CD9, CD81, CD63 (Thermo Fisher Scientific), CSPG4 and FGA (Biotech), as well as PKH26 (Red Fluorescent Cell Linker Midi Kit, Sigma).

To enhance the credibility of our results, we used three distinct human anti-TNF-α antibodies, all developed using human TNF-α as the immunogen. These antibodies are referred to here as Ab1 (Novus Biologicals, Monoclonal Mouse IgG1, Clone 6401), Ab2 (Novus Biologicals, Monoclonal Mouse IgG1, Clone 6402), and Ab3 (BD Biosciences, Monoclonal Human IgG1, κ, Clone Infliximab297.rMAb). To detect TM-TNF-α (surface), intravesical TNF-α (cargo) and total (sum of TM-TNF-α and intravesical TNF-α) TNF-α forms, we used three different staining protocols involving both unconjugated and fluorescence-conjugated antibodies:

(1) Surface TM-TNF-α: SF EVs were resuspended in df-PBS, then stained with fluorescence-conjugated TNF-α Ab1, Ab2 or Ab3 overnight at 4 °C with shaking at 400 rpm.
(2) Intravesical TNF-α: SF EVs were resuspended in df-PBS, then stained with unconjugated TNF-α Ab1, Ab2 or Ab3 for 1 h at 4 °C with shaking at 400 rpm to block surface TNF-α binding domains. SF EVs were 1:1 diluted using df-PBS and separated from the buffer using 100 kDa ultrafiltration. Next, SF EVs were fixed and permeabilized with 1 X Fixation/Permeabilization Concentrate (ThermoFisher Scientific) for 30 min on ice, followed by addition of 1 X df-Permeabilization Buffer (ThermoFisher Scientific) for 20 min at room temperature. SF EVs were separated from the buffer using 100 kDa ultrafiltration, then resuspended in 1 X df-Permeabilization Buffer and stained with the fluorescence-conjugated TNF-α Ab1, Ab2 or Ab3 overnight at 4 °C with shaking at 400 rpm.
(3) Total TNF-α: SF EVs were resuspended in 1 X Fixation/Permeabilization Concentrate for fixation, permeabilization, followed by staining with the fluorescence-conjugated TNF-α Ab1, Ab2 or Ab3 as described above.

The final volume of each sample for flow cytometric analysis was adjusted to 300 μl using df-PBS, resulting in a final dilution factor 1:10 for the original 30 μl SF used for EV separation. The flow cytometer was configured to acquire samples at around 1 μl/s acquisition volume with threshold BSC (back scatter, also known as side scatter) 0.02 % to exclude small debris particles but maintain the capacity to detect small EVs (Fig. 1A); this setting ensured that acquisition of df-PBS was below 10 events/second. Based on reference beads of mean size 100 nm (3000 Series Nanosphere™ Size Standards), 1000 nm (8000 Series Silica Particle Size Standards) and 6000 nm (Duke Standards™ 2000 Series Uniform Polymer Particles, Thermo Fisher Scientific), the relative size distribution of SF EVs were estimated and defined as follows: SEVs around 100 nm and below, MEVs 100–1000 nm, and LEVs 1000–6000

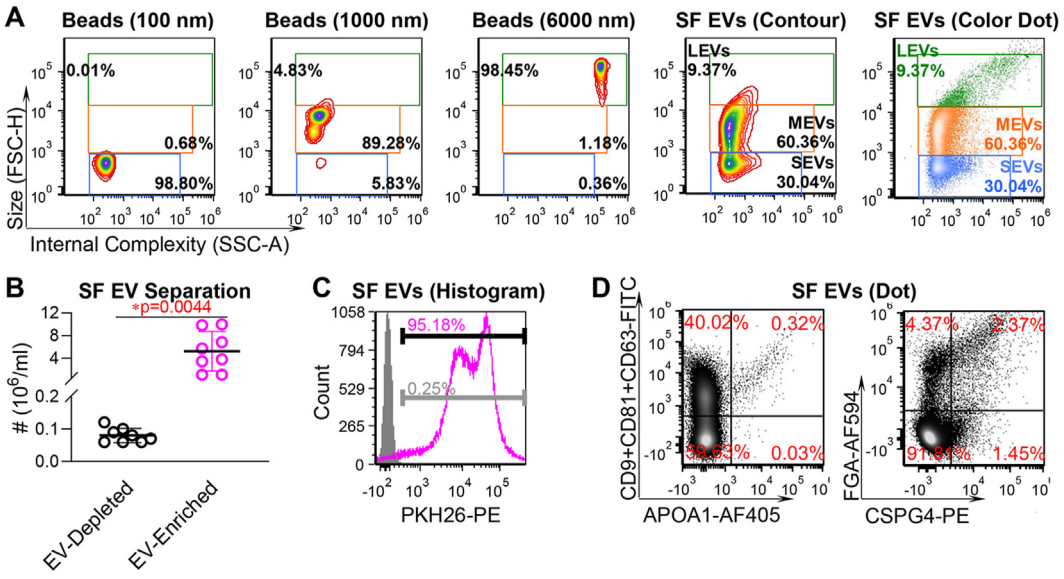

Fig. 1. OA SF EV characterization. OA SF EVs were profiled using high-resolution multicolor flow cytometry. **A**, reference beads of mean size 100, 1000 and 6000 nm were used for size estimation; the relative size distribution of SF EVs were defined as follows: LEVs, 1000–6000 nm; MEVs, 100–1000 nm; and SEVs, around 100 nm and below. The representative plots present size (FSC-H: Forward Scatter-Height), and internal complexity/granularity (SSC-A: Side Scatter-Area) for size reference beads and OA SF EVs, and the gating strategy for LEVs, MEVs and SEVs. **B**, the scatter plot displays the number of EV-depleted and EV-enriched fractions of OA SF post separation using ultrafiltration. Comparisons were performed using Paired *t*-test; significant results were defined as *p = 0.0044. **C**, the representative histogram plot displays the signal of PKH26 in unstained (grey) and stained (pink) OA SF EVs. **D**, the representative plots display the tested surface markers in OA SF EVs. (For interpretation of the references to color in this figure legend, the reader is referred to the Web version of this article.)

nm, respectively (Fig. 1A). As previously discussed [1], the estimated size range of biological vesicles is based on size reference beads and can be influenced by various factors, such as resolution and forward scatter collection angles of the flow cytometer, and the differential composition and refractive indices of the EVs and beads; therefore, the reported EV size ranges are approximate and not exact. The relative size distribution and diversity of EVs identified by different models of flow cytometers [3,11,12,14] have been corroborated by complementary techniques such as dynamic light scattering [11] and transmission electron microscopy [1].

Fluorescence compensation was calculated based on unstained and single antibody-stained UltraComp™ eBeads plus (ThermoFisher Scientific). Fluorescence background and positive signals were determined using unstained and single antibody-stained EVs and UltraComp™ eBeads plus. Percentages and mean fluorescence intensity (MFI) of EVs carrying TNF-α were determined using a high-resolution Sony MA 900 Multi-Application Sorter (Sony Biotechnology) with FCS Express 5 software (De Novo Software) for flow cytometric data analysis. The integrated mean fluorescence intensity (iMFI) was calculated by multiplying the percentage of each TNF-α^+ population with the MFI of that population [14].

2.3. Analysis of TNF Gene Expression in Various Tissue Cells

We analyzed *TNF* gene expression data in 53,961,417 human tissue cells from the CZ CELLxGENE Discover (cellxgene.cziscience.com, accessed March 03, 2025), a data platform that provides a curated data explorer for single-cell (sc) data [39]. The expression of *TNF* was determined from the available single-cell RNA sequencing (RNA-seq) data.

We also analyzed *TNF* gene expression using published scRNA-seq data from our group's study of OA joint synovium (GSE152805) [40] and additional scRNA-seq and single-nuclei (sn) RNA-seq data from another OA study of the infrapatellar fat pad and synovium (GSE216651) [41] (downloaded from the Gene Expression Omnibus on 09/20/2024). These datasets were processed and integrated [42] and *TNF* gene expression in individual patients was visualized using violin (density) plots.

2.4. Statistical analyses

GraphPad Prism 10 software (GraphPad Software) was used for statistical analyses. D'Agostino & Pearson test and Shapiro-Wilk test were used to assess data distribution. A paired *t*-test was used to compare the normally distributed number of EV-depleted and EV-enriched fractions of OA SF following ultrafiltration-based separation, with statistical significance defined as $p < 0.05$. The Friedman test with Benjamini and Hochberg multiple comparisons was used to analyze multiple groups of non-normally distributed data, including the frequencies and iMFI of the three TNF-α forms detected using three TNF-α antibodies (Ab1, Ab2, and Ab3); statistical significance was defined as an FDR value of $q < 0.05$. Spearman correlations were used to assess the associations between the frequencies detected using three TNF-α antibodies, as well as the associations between TNF-α levels and demographic variables (age and sex); statistical significance was defined as $p < 0.05$.

3. Results

3.1. OA SF EV characterization

OA SF EV populations were highly heterogeneous with a broad range of sizes, including LEVs (1000–6000 nm), MEVs (100–1000 nm), and SEVs (approximately 100 nm and smaller) (Fig. 1A), consistent with our previous observations [12,14]. Based on our previous studies [12,14], OA SF EVs display a diverse array of surface markers, including classical EV markers such as CD81, CD9, CD63, and CD29, as well as cell- and tissue-specific markers such as CD4, CD8, CD68, CD14, CD56, CD15, CD19, CD235a, CD41a, CD34, CD31, HLA-ABC, HLA-G, HLA-DRDPDQ, CSPG4, VSIG4, CD109, LRP1, BGN, CD163, MARCO, NRP1, and PTPRS. Using flow cytometry, we confirmed the efficient isolation of OA SF EVs via ultrafiltration, achieving an average 65-fold enrichment of numbers of EVs in EV-enriched fractions compared to EV-depleted fractions ($p = 0.0044$, Fig. 1B). These EV demonstrated a lipid bilayer structure as indicated by positive PKH26 signals (Fig. 1C). The EVs also expressed high frequencies of traditional EV markers (CD9, CD81 and CD63), intermediate frequencies of our novel

pathogenic OA EV markers (CSPG4 and FGA), and low frequencies of APOA1 (Fig. 1D).

3.2. Potential origin of TNF-α$^+$ EVs

Nearly all mammalian cells release EVs, contributing to a diverse pool of circulating EVs with distinct cellular and tissue origins based on their surface markers and cargo. SF is an ultrafiltrate of plasma with the addition of components from joint tissues. Our previous study showed that the amount of TNF-α$^+$ EVs in SF was positively correlated with, but dramatically higher than that in matched plasma from patients with knee OA [14]. ScRNA seq data of 53,961,417 human tissue cells from the CZ CELLxGENE Discover [39] indicates *TNF* gene expression across multiple cell types, suggesting that various tissues potentially contribute to the TNF-α$^+$ EV pool (Fig. 2A). Of note, the CZ CELLxGENE human cell atlas did not contain data on *TNF* in joint tissue chondrocytes or synoviocytes. We therefore evaluated RNA-seq data resources to help determine the potential joint tissue contributors to the pool of TNF-α$^+$ EVs in SF. Our scRNA-seq data (GSE152805) [40] indicated that the *TNF* gene was expressed by 16 % of synoviocytes, predominantly inflammatory macrophages and other HLA-DR$^+$ cells, but less than 1 % of chondrocytes. A complementary study (GSE216651) also identified inflammatory macrophages as a major source of *TNF* in the synovium and infrapatellar fat pad [41]. Visualization of *TNF* expression across these datasets (Fig. 2B) suggests synoviocytes as key contributors to TNF-α$^+$ EVs in OA SF.

3.3. OA SF EVs contain both transmembrane and intravesical TNF-α

Both TM-TNF-α and intravesical TNF-α were detected in all EV size subsets (LEVs, MEVs, SEVs) of OA SF (Fig. 3). The mean percentages of TNF-α detected in SF EVs using three different antibodies were as follows: TM-TNF-α 2.26 %, 4.74 % and 0.69 %; intravesical TNF-α 11.86 %, 11.98 % and 2 %; and total TNF-α 20.62 %, 18.18 % and 4.46 % (Fig. 4). The median percentages of TNF-α detected in SF EVs using the three different antibodies were as follows: TM-TNF-α 1.07 %, 2.98 % and 0.55 %; intravesical TNF-α 9.83 %, 6.62 % and 1.93 %; and total TNF-α 18.90 %, 16.54 % and 2.69 %. A q value below a threshold 0.05 was considered statistically significant (Fig. 4). These frequencies of TM-TNF-α on OA SF EVs are similar to those observed on many peripheral blood immune cells, such as neutrophils, T cells, B cells and nature killer cells [31]. Based on both percentage (reflecting the frequency) and iMFI (reflecting the frequency and intensity), flow cytometric analysis confirmed that TM-TNF-α was present on OA SF EVs, though it was less abundant than intravesical TNF-α, with consistent results across all three antibodies (median percentages 1.07 % vs. 9.83 %, 2.98 % vs. 6.62 % and 0.55 % vs. 1.93 %; $q < 0.05$, Fig. 4). Notably, while our previous study identified significant Spearman correlations between certain OA SF EV peptides and demographic variables [12], we did not observe any significant Spearman correlations between the percentage or iMFI of any TNF-α forms in OA SF EVs and age or sex ($p > 0.05$, data not shown).

Notably, the three TNF-α antibodies detected different frequencies of TM-TNF-α, intravesical TNF-α, and total TNF-α in OA SF EVs (Fig. 5, Fig. 6A, $q < 0.05$), consistent with previous findings that anti-TNF agents exhibit differential affinities, avidities, and effects on soluble and transmembrane TNF-α, as well as TNF-α-producing cells [16,32,35]. Despite these differences, the TNF-α$^+$ SF EV frequencies detected by all three antibodies were generally correlated (Fig. 6B).

4. Discussion

Our previous study identified plasma EV-associated TNF-α concentrations and the frequencies of TNF-α$^+$ LEV, MEV, and SEV subpopulations as individual predictors of knee rOA progression [10]. While these findings implicate TNF-α in OA pathogenesis [10,43], the failure of

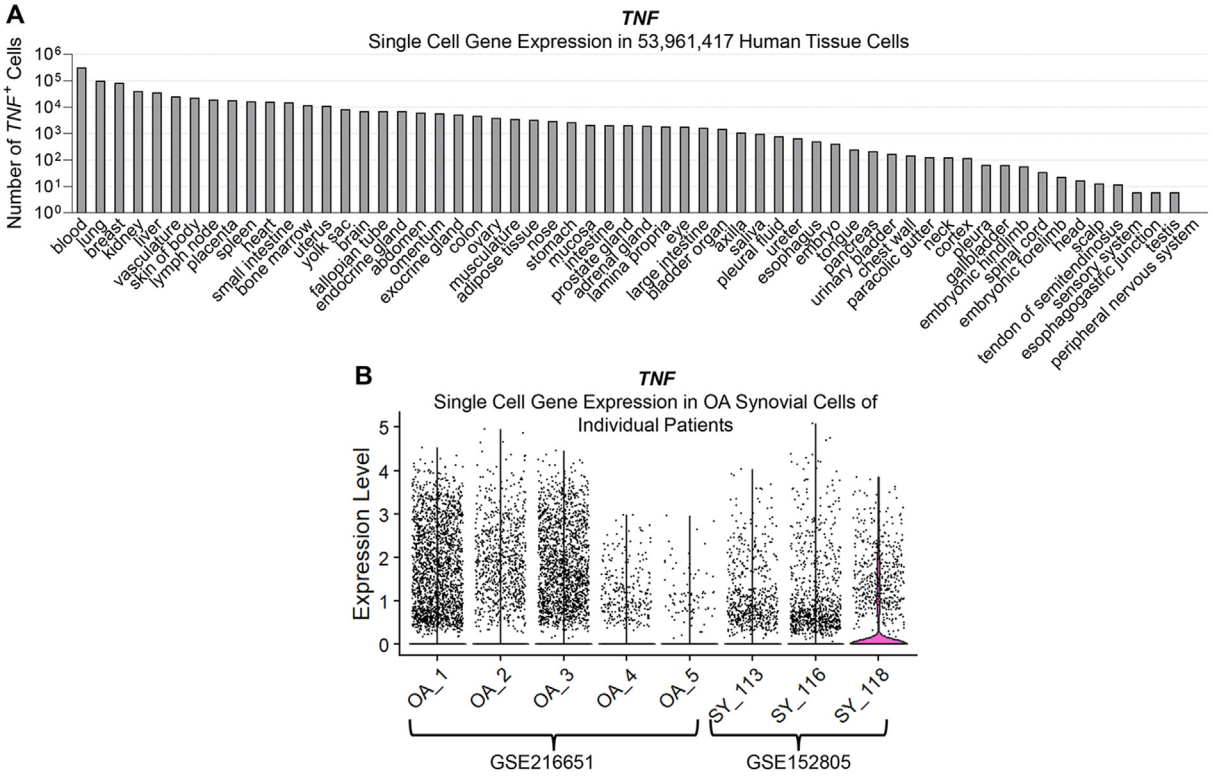

Fig. 2. TNF Gene Expression in Various Tissue Cells. A, scRNA seq data of 53,961,417 human tissue cells from the CZ CELLxGENE Discover revealed the number of *TNF*$^+$cells in the indicated human tissue. **B**, scRNA-seq data of OA joint synovium from our group (GSE152805) and scRNA-seq and snRNA-seq data of OA joint infrapatellar fat pad and synovium from another OA study (GSE216651) were processed and merged, and *TNF* gene expression in individual patients was visualized using the violin plots. Both datasets show strong expressions of *TNF*.

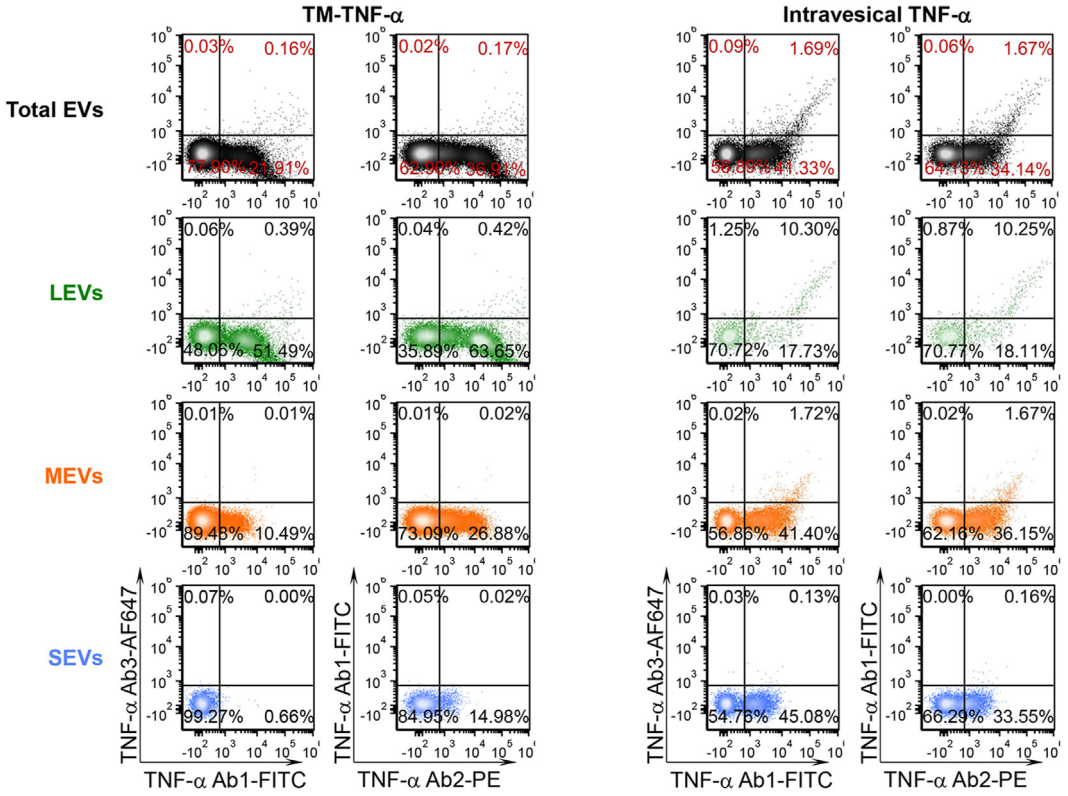

Fig. 3. Both TM-TNF-α and intravesical TNF-α were detected in LEVs, MEVs, and SEVs of OA SF. OA SF EVs were profiled for TM-TNF-α$^+$ and intravesical TNF-α$^+$ SF EVs (see Methods) using high-resolution multicolor flow cytometry. The representative color plots display the signal of TM-TNF-α and intravesical TNF-α in total SF EVs and gated LEVs, MEVs and SEVs. (For interpretation of the references to color in this figure legend, the reader is referred to the Web version of this article.)

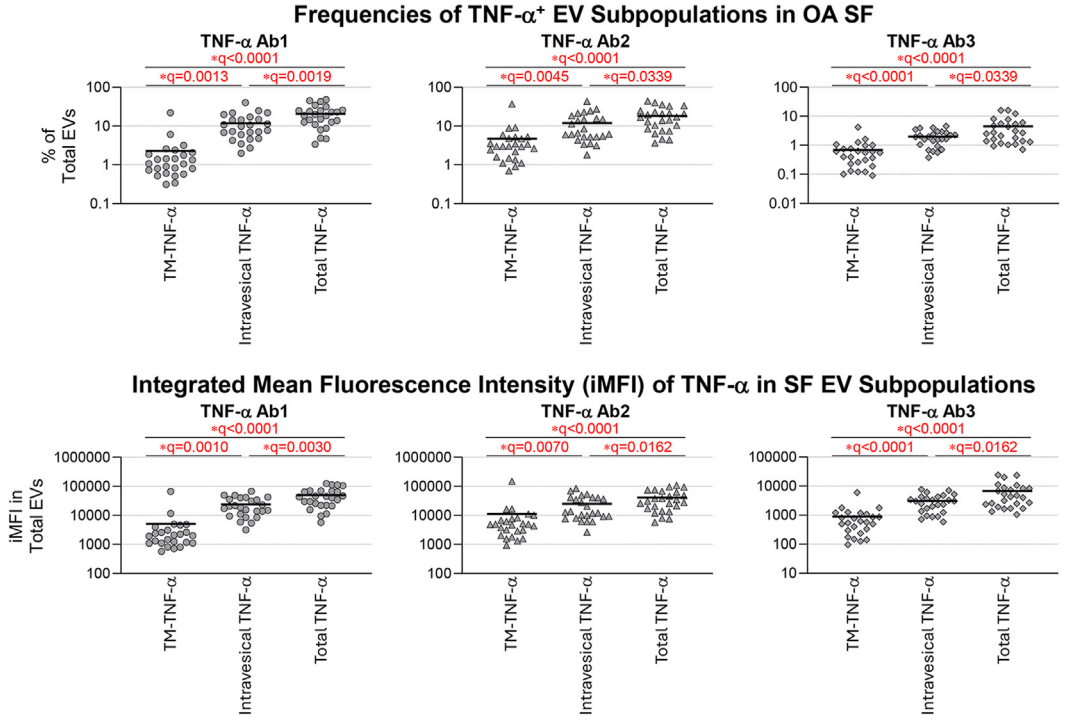

Fig. 4. The frequency and iMFI of TM-TNF-α was lower than intravesical TNF-α in OA SF EVs. SF EVs from patients with knee OA (n = 25) were profiled for TM-TNF-α$^+$, intravesical TNF-α$^+$ and total TNF-α$^+$ SF EVs using three different anti-TNF-α antibodies and three staining protocols (see methods), followed by analyses using high-resolution multicolor flow cytometry. The scatterplots represent the percentage of TM-TNF-α$^+$, intravesical TNF-α$^+$ and total TNF-α$^+$ SF EV subpopulations and the iMFI of the three TNF-α forms. Comparisons were performed using Friedman test with Benjamini and Hochberg multiple comparisons; significant results were defined as FDR value * $q < 0.05$.

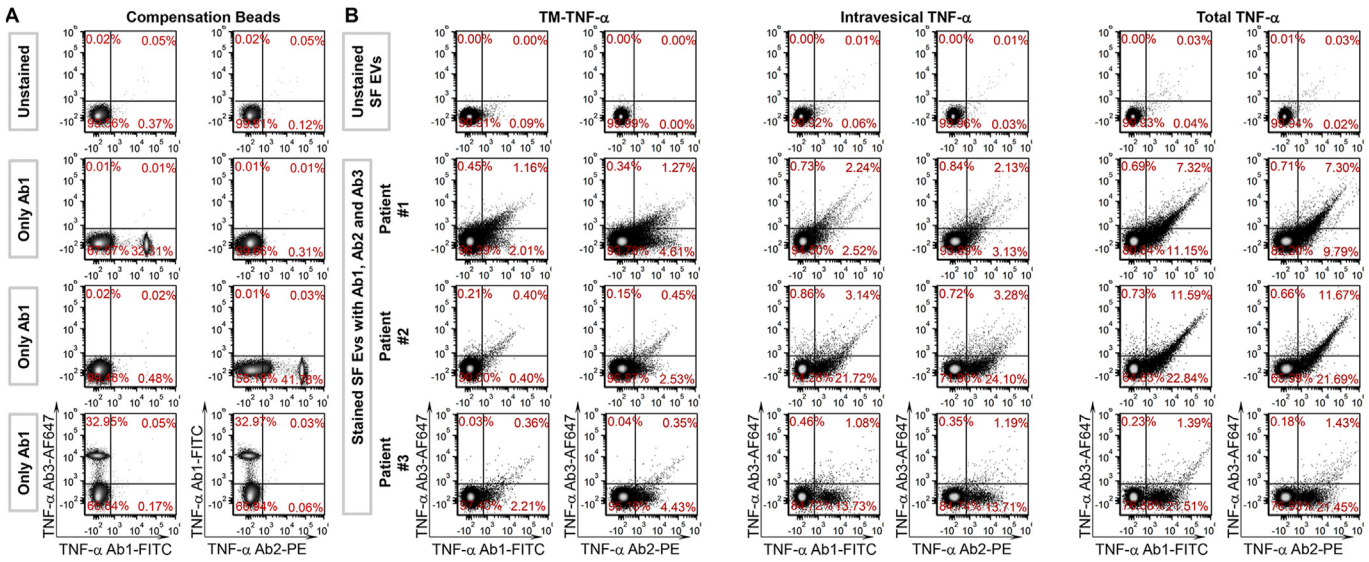

Fig. 5. The profile of TM-TNF-α$^+$, intravesical TNF-α$^+$ and total TNF-α$^+$ EVs in OA SF. A, the fluorescence compensation was adjusted based on the unstained and single antibody-stained compensation beads. The representative plots display the negative and positive signal of each channel. **B**, the representative plots display the negative background determined using unstained SF EVs, and the percentage of TM-TNF-α$^+$, intravesical TNF-α$^+$ and total TNF-α$^+$ EV subpopulations in stained SF EVs from 3 individual patients with knee OA.

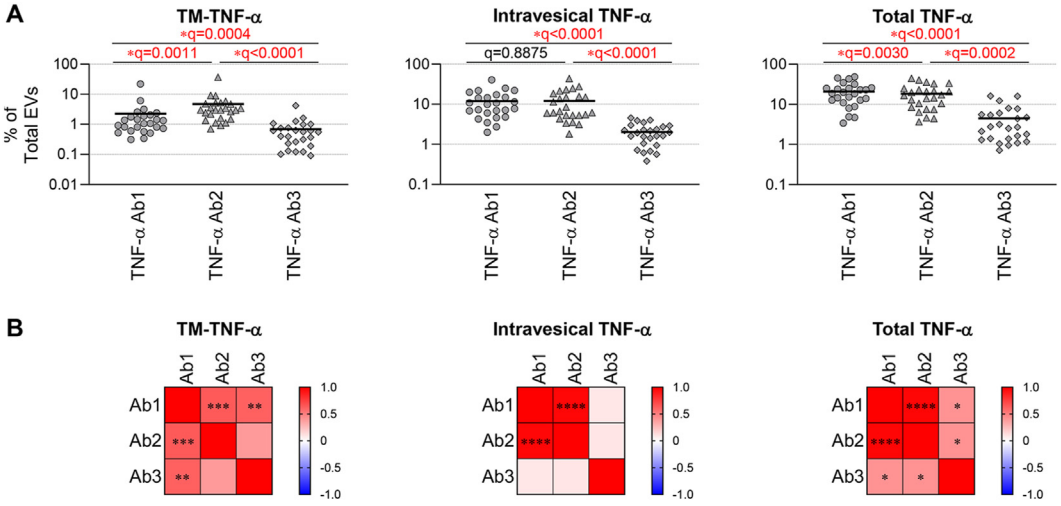

Fig. 6. Three TNF-α antibodies detected different frequencies of TM-TNF-α, intravesical TNF-α and total TNF-α in OA SF EVs. SF EVs from patients with knee OA (n = 25) were profiled for TM-TNF-α$^+$, intravesical TNF-α$^+$ and total TNF-α$^+$ SF EVs using three different anti-TNF-α antibodies. **A**, the scatter plots display the frequencies of TM-TNF-α, intravesical TNF-α and total TNF-α in OA SF EVs detected using three TNF-α antibodies. Comparisons were performed using Friedman test with Benjamini and Hochberg multiple comparisons; significant results were defined as FDR value * $q < 0.05$. **B**, Spearman correlations were used to assess associations of the frequencies detected with the three TNF-α antibodies; heat maps depict the Spearman correlation coefficient r values; significant results were defined as * $p < 0.05$, ** $p < 0.01$, *** $p < 0.001$ and **** $p < 0.0001$.

anti-TNF-α biologics in OA trials raises questions about the role of EV-associated TNF-α in OA. In this study, we established that OA SF EVs carry TNF-α, both on their lipid bilayer (TM-TNF-α) and as intravesical cargo. Interestingly, the amount of TM-TNF-α on the surface of EVs was comparable to that found on several major immune cell subsets in peripheral blood [31].

TM-TNF-α is known to induce arthritis in mouse models [32], and by analogy to cells, TM-TNF-α on EVs may bind to TNF receptors on target cells, triggering pro-inflammatory signaling. Additionally, some EVs can fuse to the plasma membrane or endosome of recipient cells, releasing their cargo into the recipient cells' cytosol, and integrate their membrane proteins, including TM-TNF-α, into the recipient cell membranes [3,44]. This transfer enables TM-TNF-α to function both as a ligand and receptor, transmitting outside-to-inside (reverse) signals to host cells upon TNF receptor binding [32]. Given that anti-TNF agents have lower affinities for TM-TNF-α compared to soluble TNF-α [16,32], EV associated TNF-α may contribute to OA pathogenesis while evading neutralization due to lower affinity for anti-TNF-α therapeutics and/or sequestration within EVs. Further investigation is needed to determine the distinct roles of TM-TNF-α and intravesical TNF-α in OA, and to determine the optimal strategy for blocking EV-associated TNF-α in conjunction with soluble TNF-α.

A strength of our study was the use of three different anti-TNF-α antibodies to validate the presence and quantity of TM-TNF-α on SF EVs, minimizing the likelihood of spurious identification due to antibody cross-reactivity with other molecules. Although we previously observed robust uptake of EVs by recipient cells and transfer of EV membranes (PKH26 labeled) to recipient cells [3], further research is needed to

evaluate the transfer of EV-bound TNF-α (TM-TNF-α and intravesical TNF-α) to recipient cells, and elucidate the functional consequences of this transfer.

A key limitation of our study is that all SF samples were acquired as anonymized waste specimens at the time of therapeutic aspiration of effusion of individuals with knee rOA or TKR for OA, for which we did not have access to medical records. Consequently, in this study we were unable to assess the relationship between SF EV TNF-α and disease severity or degree of knee inflammation. However, addressing these limitations remains a priority for future research.

In summary, EV-bound TNF-α appears to be pathogenic while being relatively inaccessible to current TNF-α inhibitors. These findings may help explain the limited success of TNF-α inhibitors in OA trials and provide a foundation for exploring alternative therapeutic approaches, such as targeting EVs carrying TM-TNF-α and intravesical TNF-α or increasing the local concentrations of TNF-α inhibitors via intra-articular injection.

Informed consent statement

All SF samples were acquired as anonymized waste specimens under the approval of the Institutional Review Board of Duke University.

Author contributions

Conceptualization, X.Z. and V.B.K.; methodology, X.Z.; validation, X.Z.; formal analysis, X.Z.; investigation, X.Z.; resources, V.B.K.; data curation, X.Z.; writing—original draft preparation, X.Z.; writing—review and editing, X.Z. and V.B.K; visualization, X.Z.; supervision, V.B.K.; project administration, X.Z. and V.B.K.; funding acquisition, X.Z. and V.B.K. All authors have read and agreed to the published version of the manuscript.

Institutional review board statement

This study was reviewed and approved by the Institutional Review Board of Duke University (Pro00010301 and Pro00008622) and was conducted in compliance with relevant guidelines.

Data availability statement

All data used to evaluate the conclusions in the paper are present in the paper and/or the Supplementary Materials.

Role of the funding source

This research was funded by the National Institute on Aging, grant numbers R01AG070146 (VBK, XZ).

Declaration of competing interest

XZ and VBK have a patent pending related to EV predictors of OA severity and progression.

Acknowledgments

The authors wish to acknowledge all participants who donated specimens for this study; Jason Jinkun Tao for processing, analyzing and visualizing single-cell RNA sequencing and single-nuclei RNA sequencing data; Janet L Huebner for specimen management; the Duke Cancer Institute Flow Cytometry Shared Resource for providing access to the Sony MA 900 Multi-Application Sorter; the Duke Human Vaccine Institute Research Flow Cytometry Shared Resource Facility for providing the FCS Express 5 software.

References

[1] X. Zhang, G.S. Baht, R. Huang, Y.H. Chen, K.H. Molitoris, S.E. Miller, et al., Rejuvenation of neutrophils and their extracellular vesicles is associated with enhanced aged fracture healing, Aging Cell 21 (2022) e13651.
[2] M.A. Thomas, M.J. Fahey, B.R. Pugliese, R.M. Irwin, M.A. Antonyak, M.L. Delco, Human mesenchymal stromal cells release functional mitochondria in extracellular vesicles, Front. Bioeng. Biotechnol. 10 (2022) 870193.
[3] X. Zhang, S. Ma, J.L. Huebner, S.I. Naz, N. Alnemer, E.J. Soderblom, et al., Immune system-related plasma extracellular vesicles in healthy aging, Front. Immunol. 15 (2024) 1355380.
[4] J. Sanz-Ros, C. Mas-Bargues, N. Romero-Garcia, J. Huete-Acevedo, M. Dromant, C. Borras, The potential use of mitochondrial extracellular vesicles as biomarkers or therapeutical tools, Int. J. Mol. Sci. 24 (2023).
[5] Z. She, M. Xie, M. Hun, A.S. Abdirahman, C. Li, F. Wu, et al., Immunoregulatory effects of mitochondria transferred by extracellular vesicles, Front. Immunol. 11 (2020) 628576.
[6] C. Admyre, B. Bohle, S.M. Johansson, M. Focke-Tejkl, R. Valenta, A. Scheynius, et al., B cell-derived exosomes can present allergen peptides and activate allergen-specific T cells to proliferate and produce TH2-like cytokines, J. Allergy Clin. Immunol. 120 (2007) 1418–1424.
[7] H. Valadi, K. Ekstrom, A. Bossios, M. Sjostrand, J.J. Lee, J.O. Lotvall, Exosome-mediated transfer of mRNAs and microRNAs is a novel mechanism of genetic exchange between cells, Nat. Cell Biol. 9 (2007) 654–659.
[8] R. Domenis, R. Zanutel, F. Caponnetto, B. Toffoletto, A. Cifu, C. Pistis, et al., Characterization of the proinflammatory profile of synovial fluid-derived exosomes of patients with osteoarthritis, Mediat. Inflamm. 2017 (2017) 4814987.
[9] K. Gao, W. Zhu, H. Li, D. Ma, W. Liu, W. Yu, et al., Association between cytokines and exosomes in synovial fluid of individuals with knee osteoarthritis, Mod. Rheumatol. 30 (2020) 758–764.
[10] X. Zhang, M.F. Hsueh, J.L. Huebner, V.B. Kraus, TNF-Alpha carried by plasma extracellular vesicles predicts knee osteoarthritis progression, Front. Immunol. 12 (2021) 758386.
[11] X. Zhang, M.J. Hubal, V.B. Kraus, Immune cell extracellular vesicles and their mitochondrial content decline with ageing, Immun. Ageing 17 (2020) 1.
[12] X. Zhang, S. Ma, S.I. Naz, V. Jain, E.J. Soderblom, C. Aliferis, et al., Comprehensive characterization of pathogenic synovial fluid extracellular vesicles from knee osteoarthritis, Clin. Immunol. 257 (2023) 109812.
[13] Z. Li, M. Li, P. Xu, J. Ma, R. Zhang, Compositional variation and functional mechanism of exosomes in the articular microenvironment in knee osteoarthritis, Cell Transplant. 29 (2020) 963689720968495.
[14] X. Zhang, J.L. Huebner, V.B. Kraus, Extracellular vesicles as biological indicators and potential sources of autologous therapeutics in osteoarthritis, Int. J. Mol. Sci. 22 (2021).
[15] D. Sokolov, A. Gorshkova, E. Tyshchuk, P. Grebenkina, M. Zementova, I. Kogan, et al., Large extracellular vesicles derived from natural killer cells affect the functions of monocytes, Int. J. Mol. Sci. 25 (2024).
[16] Z. Kaymakcalan, P. Sakorafas, S. Bose, S. Scesney, L. Xiong, D.K. Hanzatian, et al., Comparisons of affinities, avidities, and complement activation of adalimumab, infliximab, and etanercept in binding to soluble and membrane tumor necrosis factor, Clin. Immunol. 131 (2009) 308–316.
[17] E. Chisari, K.M. Yaghmour, W.S. Khan, The effects of TNF-alpha inhibition on cartilage: a systematic review of preclinical studies, Osteoarthr. Cartil. 28 (2020) 708–718.
[18] A.Y. Guzelant, M. Isyar, I. Yilmaz, D.Y. Sirin, S. Cakmak, M. Mahirogullari, Are chondrocytes damaged when rheumatologic inflammation is suppressed? Drug Chem. Toxicol. 40 (2017) 13–23.
[19] M. Isyar, B. Bilir, I. Yilmaz, S. Cakmak, D.Y. Sirin, A.Y. Guzelant, et al., Are biological agents toxic to human chondrocytes and osteocytes? J. Orthop. Surg. Res. 10 (2015) 118.
[20] S. Zigon-Branc, A. Barlic, M. Knezevic, M. Jeras, G. Vunjak-Novakovic, Testing the potency of anti-TNF-alpha and anti-IL-1beta drugs using spheroid cultures of human osteoarthritic chondrocytes and donor-matched chondrogenically differentiated mesenchymal stem cells, Biotechnol. Prog. 34 (2018) 1045–1058.
[21] K.A. Elsaid, J.T. Machan, K. Waller, B.C. Fleming, G.D. Jay, The impact of anterior cruciate ligament injury on lubricin metabolism and the effect of inhibiting tumor necrosis factor alpha on chondroprotection in an animal model, Arthritis Rheum. 60 (2009) 2997–3006.
[22] A. Kawaguchi, H. Nakaya, T. Okabe, K. Tensho, M. Nawata, Y. Eguchi, et al., Blocking of tumor necrosis factor activity promotes natural repair of osteochondral defects in rabbit knee, Acta Orthop. 80 (2009) 606–611.
[23] M.S. Linn, D.C. Chase, R.M. Healey, F.L. Harwood, W.D. Bugbee, D. Amiel, Etanercept enhances preservation of osteochondral allograft viability, Am. J. Sports Med. 39 (2011) 1494–1499.
[24] C.H. Ma, Q. Lv, Y.X. Yu, Y. Zhang, D. Kong, K.R. Niu, et al., Protective effects of tumor necrosis factor-alpha blockade by adalimumab on articular cartilage and subchondral bone in a rat model of osteoarthritis, Braz. J. Med. Biol. Res. 48 (2015) 863–870.
[25] R. Ossendorff, S. Grad, M.J. Stoddart, M. Alini, H. Schmal, N. Sudkamp, et al., Autologous chondrocyte implantation in osteoarthritic surroundings: TNFalpha and its inhibition by adalimumab in a knee-specific bioreactor, Am. J. Sports Med. 46 (2018) 431–440.
[26] D.J. Shealy, P.H. Wooley, E. Emmell, A. Volk, A. Rosenberg, G. Treacy, et al., Anti-TNF-alpha antibody allows healing of joint damage in polyarthritic transgenic mice, Arthritis Res. 4 (2002) R7.

[27] D.M. Urech, U. Feige, S. Ewert, V. Schlosser, M. Ottiger, K. Polzer, et al., Anti-inflammatory and cartilage-protecting effects of an intra-articularly injected anti-TNFalpha single-chain Fv antibody (ESBA105) designed for local therapeutic use, Ann. Rheum. Dis. 69 (2010) 443–449.
[28] H. Yang, M. Zhang, X. Wang, H. Zhang, J. Zhang, L. Jing, et al., TNF accelerates death of mandibular condyle chondrocytes in rats with biomechanical stimulation-induced temporomandibular joint disease, PLoS One 10 (2015) e0141774.
[29] Q. Zhang, H. Lv, A. Chen, F. Liu, X. Wu, Efficacy of infliximab in a rabbit model of osteoarthritis, Connect. Tissue Res. 53 (2012) 355–358.
[30] J. Zwerina, S. Hayer, M. Tohidast-Akrad, H. Bergmeister, K. Redlich, U. Feige, et al., Single and combined inhibition of tumor necrosis factor, interleukin-1, and RANKL pathways in tumor necrosis factor-induced arthritis: effects on synovial inflammation, bone erosion, and cartilage destruction, Arthritis Rheum. 50 (2004) 277–290.
[31] X. Zhou, S. Zhou, B. Li, Q. Li, L. Gao, D. Li, et al., Transmembrane TNF-alpha preferentially expressed by leukemia stem cells and blasts is a potent target for antibody therapy, Blood 126 (2015) 1433–1442.
[32] T. Horiuchi, H. Mitoma, S. Harashima, H. Tsukamoto, T. Shimoda, Transmembrane TNF-alpha: structure, function and interaction with anti-TNF agents, Rheumatology 49 (2010) 1215–1228.
[33] M. Kriegler, C. Perez, K. DeFay, I. Albert, S.D. Lu, A novel form of TNF/cachectin is a cell surface cytotoxic transmembrane protein: ramifications for the complex physiology of TNF, Cell 53 (1988) 45–53.
[34] E. Decoster, B. Vanhaesebroeck, P. Vandenabeele, J. Grooten, W. Fiers, Generation and biological characterization of membrane-bound, uncleavable murine tumor necrosis factor, J. Biol. Chem. 270 (1995) 18473–18478.
[35] H. Mitoma, T. Horiuchi, H. Tsukamoto, Y. Tamimoto, Y. Kimoto, A. Uchino, et al., Mechanisms for cytotoxic effects of anti-tumor necrosis factor agents on transmembrane tumor necrosis factor alpha-expressing cells: comparison among infliximab, etanercept, and adalimumab, Arthritis Rheum. 58 (2008) 1248–1257.
[36] J.A. Welsh, D.C.I. Goberdhan, L. O'Driscoll, E.I. Buzas, C. Blenkiron, B. Bussolati, et al., Minimal information for studies of extracellular vesicles (MISEV2023): from basic to advanced approaches, J. Extracell. Vesicles 13 (2024) e12404.
[37] D.E. Jimenez, M. Tahir, M. Faheem, W. Alves, B.L. Correa, G.R. Andrade, et al., Comparison of four purification methods on serum extracellular vesicle recovery, size distribution, and proteomics, Proteomes 11 (2023).
[38] F. Aliakbari, N.B. Stocek, M. Cole-Andre, J. Gomes, G. Fanchini, S.H. Pasternak, et al., A methodological primer of extracellular vesicles isolation and characterization via different techniques, Biol Methods Protoc 9 (2024) bpae009.
[39] CZI Cell Science Program, S. Abdulla, B. Aevermann, P. Assis, S. Badajoz, S.M. Bell, E. Bezzi, et al., CZ CELLxGENE Discover: a single-cell data platform for scalable exploration, analysis and modeling of aggregated data, Nucleic Acids Res. 53 (2025) D886–D900.
[40] C.H. Chou, V. Jain, J. Gibson, D.E. Attarian, C.A. Haraden, C.B. Yohn, et al., Synovial cell cross-talk with cartilage plays a major role in the pathogenesis of osteoarthritis, Sci. Rep. 10 (2020) 10868.
[41] Chanzuckerberg Initiative, CZ CELLxGENE discover, 2022. Retrieved (2022), from https://cellxgene.cziscience.com/.
[42] A. Butler, P. Hoffman, P. Smibert, E. Papalexi, R. Satija, Integrating single-cell transcriptomic data across different conditions, technologies, and species, Nat. Biotechnol. 36 (2018) 411–420.
[43] J. Xue, J. Wang, Q. Liu, A. Luo, Tumor necrosis factor-alpha induces ADAMTS-4 expression in human osteoarthritis chondrocytes, Mol. Med. Rep. 8 (2013) 1755–1760.
[44] C. Wan, M.H.B. Stowell, J. Shen, Progress and gaps of extracellular vesicle-mediated intercellular cargo transfer in the central nervous system, Commun. Biol. 5 (2022) 1223.